

Topology-Controlled Nonreciprocal Photon Scattering in a Waveguide

Wei Nie,^{1,2,3} Tao Shi,^{4,5,*} Franco Nori,^{3,6} and Yu-xi Liu^{1,2,†}

¹*Institute of Microelectronics, Tsinghua University, Beijing 100084, China*

²*Frontier Science Center for Quantum Information, Beijing, China*

³*Theoretical Quantum Physics Laboratory, RIKEN Cluster for Pioneering Research, Wako-shi, Saitama 351-0198, Japan*

⁴*Institute of Theoretical Physics, Chinese Academy of Sciences, P.O. Box 2735, Beijing 100190, China*

⁵*CAS Center for Excellence in Topological Quantum Computation,*

University of Chinese Academy of Sciences, Beijing 100049, China

⁶*Physics Department, The University of Michigan, Ann Arbor, Michigan 48109-1040, USA*

Waveguide quantum electrodynamics with multiple atoms provides an important way to study photon transport. In this work, we study the photon transport in a one-dimensional waveguide coupled to a topological atom array. The interaction between light and topology-dressed atoms yields a rich variety of photon scattering phenomena. We find that the nonreciprocal photon reflection originates from the quantum interference of photons scattered by the dissipative edge and bulk modes in the topological atom array. The largest nonreciprocity is found at the magic atomic spacing $d = 3\lambda_0/4$, where λ_0 is the characteristic wavelength of the waveguide. For an odd number of atoms with an extremely small free space decay, the broken inversion and time-reversal symmetries induce a giant anomalous photon loss from the waveguide to free space. Our model can be implemented in superconducting quantum circuits. This work opens a new avenue to manipulate photons via the interaction between light and topological quantum matter.

Introduction.—One-dimensional (1D) waveguides are essential light-matter interfaces and have fundamental applications in quantum devices and quantum networks [1–3]. The photon transport in a waveguide can be controlled by coupling to a single atom [4–24] or an atom array [25–33]. In the subwavelength regime, the interference of photons emitted from atoms at different positions [34–37] gives rise to the collective enhancement of photon transport [38–42] and directional photon emission [43–45]. In waveguide quantum electrodynamics (QED) systems, e.g., atoms trapped around nanofibers [46–50], the direct atom-atom interaction is in general negligible. However, the direct interaction between atoms is essential in superconducting quantum circuits. By engineering this interaction, one can simulate many models in condensed matter physics and high energy physics, including spin models [51–53], topological matter [54–56], and lattice gauge theories [57, 58].

Of particular interest, symmetry-protected topological phases of matter open a field in materials science [59], and provide extensive opportunities in quantum computation and information technology [60–65]. In 2008, Refs. [66, 67] proposed to manipulate photon transport using topology, which paved the way for topological photonics [68–72]. In 2D or higher dimensional topological materials, photons can be guided via channels supported by edge modes and surface modes [73–77]. Such transport is immune to imperfections, randomness, and disorder due to the large bandgap separating chiral edge modes and bulk modes. The topological protection of photon transport has been realized in different incarnations of optical systems [78–83].

In this Letter, by virtue of the interaction between light and topological atom array via a waveguide, we

show the intriguing photon scattering induced by the nontrivial topology. Arrays with an odd number of equally spaced atoms are described by the Su-Schrieffer-Heeger (SSH) model [84], as shown in Fig. 1(a). We find that for a magic atomic spacing d , in contrast to the reciprocal transmission the reflection

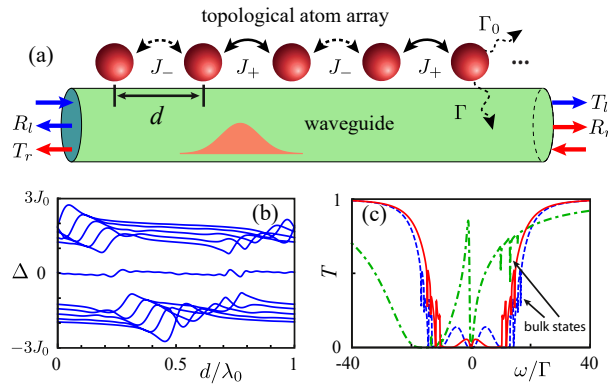


FIG. 1. (a) Schematic of a 1D waveguide coupled to a topological atom array. The dimerized interactions are $J_{\mp} = J_0(1 \mp \cos \varphi)$. Here we consider an array with an odd number of atoms and $0 \leq \varphi < \pi/2$. Thus, an edge state is localized to left edge of the atom array. A homogenous spacing d is assumed for neighboring atoms along the waveguide. All the atoms have decays to the waveguide and free space, denoted by Γ and Γ_0 . T_l (T_r) and R_l (R_r) represent the transmission and reflection for the left- (right-) incident photon, respectively. (b) Real energy spectrum of the effective Hamiltonian H_{eff} . The edge state is protected from bulk states by the bandgap. (c) Transmission spectra $T = |t(\omega)|^2$ for $d = \lambda_0/4$ (blue-dashed), $d = \lambda_0/2$ (green-dotdashed) and $d = 3\lambda_0/4$ (red-solid). Dips around $\omega = \pm 2J_0$ indicate bulk states. In (b) and (c), we consider $J_0/\Gamma = 8$, $\varphi = 0.3\pi$ and atom number $N = 11$.

is nonreciprocal. This is attributed to the interplay between the inversion symmetry breaking induced by the non-trivial topology and the time-reversal symmetry breaking due to dissipation. More precisely, the quantum interference of electromagnetic waves reflected by the dissipative edge and bulk states gives rise to the *large nonreciprocity*. We propose the implementation of our model in superconducting quantum circuits.

Single-photon scattering by a topological atom array.—As shown in the schematic Fig. 1(a), we study a topological atom array coupled to photonic modes in a 1D waveguide with linear dispersion. The Hamiltonian of the waveguide is ($\hbar \equiv 1$)

$$H_{\text{wg}} = -ic \int dx \left(\hat{a}_r^\dagger(x) \frac{\partial}{\partial x} \hat{a}_r(x) - \hat{a}_l^\dagger(x) \frac{\partial}{\partial x} \hat{a}_l(x) \right), \quad (1)$$

where \hat{a}_l^\dagger (\hat{a}_r^\dagger) and \hat{a}_l (\hat{a}_r) are the creation and annihilation operators for the left (right) propagating photons, respectively. The topological atom array is described by the SSH model [84]

$$H_{\text{ssh}} = \left(J_- \sum_{i=\text{odd}} \sigma_i^+ \sigma_{i+1}^- + J_+ \sum_{i=\text{even}} \sigma_i^+ \sigma_{i+1}^- \right) + \text{H.c.}, \quad (2)$$

where $\sigma_i^+ = |e_i\rangle\langle g_i|$ depicts the transition from the ground state $|g_i\rangle$ to the excited state $|e_i\rangle$ of the i -th atom, and the nearest neighbor flip-flop interactions change alternatively along the chain as $J_\mp = J_0(1 \mp \cos \varphi)$. Different from the two edge modes in the SSH lattice with even number of sites [85], only a single edge state exists at either the left ($0 \leq \varphi < \pi/2$) or the right ($\pi/2 < \varphi \leq \pi$) boundary of the topological array with an odd number of sites. Without loss of generality, we focus on the atom array with a left-localized edge state, i.e., $0 \leq \varphi < \pi/2$.

The interaction $H_{\text{int}} = g \sum_{i,\alpha=l,r} \hat{a}_\alpha^\dagger(x_i) \sigma_i^- e^{-is_\alpha k_0 x_i} + \text{H.c.}$ between atoms and the waveguide is determined by the coupling strength g and the wave vector $k_0 = \omega_0/c$, where $s_\alpha = \pm$ for the right- and left-moving photons, and ω_0 and x_i are the transition frequency and the position of the i th atom. The photons in the waveguide mediate the long-range interaction of atoms and induce the collective dissipation [34, 86]. By integrating out the photonic modes, we obtain the non-Hermitian effective Hamiltonian

$$H_{\text{eff}} = H_{\text{ssh}} + H'_{\text{fs}} + H'_{\text{w}}, \quad (3)$$

under the Markovian approximation. Here, $H'_{\text{fs}} = -i\Gamma_0 \sum_i \sigma_i^+ \sigma_i^-$, with Γ_0 being the decay rate to free space, and $H'_{\text{w}} = -i\Gamma \sum_{i,j} e^{ik_0|x_i-x_j|} \sigma_i^+ \sigma_j^-$, where $\Gamma = g^2/c$ denotes the spontaneous emission rate to the waveguide. The interplay of the coherent dynamics governed by the SSH Hamiltonian H_{ssh} and the incoherent interaction H'_{w} determines the topological features. One can expect in the strong coherent coupling

regime, i.e., $J_0 \gg \Gamma$, that the localized edge state survives. In Fig. 1(b), we show the real part $\Delta = \text{Re}(E)$ of the energy spectrum E of H_{eff} for $J_0 \gg \Gamma$. The spectrum has the periodicity $\lambda_0 = 2\pi/k_0$ in d . As d varies from 0 to λ_0 , the spectrum of bulk states is significantly changed due to the long-range interaction mediated by waveguide photons [50]. However, since the edge state is topologically protected from the bulk modes by the bandgap, it is only slightly shifted. In particular, both the left and right halves of the spectrum have the rotational symmetry by π with respect to $(d, \Delta) = (\lambda_0/4, 0)$ and $(3\lambda_0/4, 0)$, respectively.

Compared with the optical responses [34, 35] of the atom array without direct interaction, i.e., $J_0 = 0$, the topological atom array has a profound influence on the photon transport. For a single photon with frequency $\omega = ck$, the transmission and reflection amplitudes can be obtained as [87]

$$t(\omega) = 1 - i\Gamma \sum_j \frac{\mathbf{V}^\dagger |\psi_j^R\rangle \langle \psi_j^L| \mathbf{V}}{\omega - \Delta_j + i\Gamma_j}, \quad (4)$$

$$r(\omega) = -i\Gamma \sum_j \frac{\mathbf{V}^T |\psi_j^R\rangle \langle \psi_j^L| \mathbf{V}}{\omega - \Delta_j + i\Gamma_j}, \quad (5)$$

where $\mathbf{V} = (e^{\pm ik_0 x_1}, e^{\pm ik_0 x_2}, \dots)^T$ for the left- and right-incident photons, respectively, and the right and left eigenvectors $|\psi_j^R\rangle$ and $|\psi_j^L\rangle$ of H_{eff} Eq. (3) form the biorthogonal basis, i.e., $\langle \psi_j^L | \psi_j^R \rangle = \delta_{jj'}$ [88]. The real and imaginary parts of E , i.e., Δ_j and $\Gamma_j = -\text{Im}(E_j)$, denote the energy shift and the effective decay of the j th mode in H_{eff} , respectively. And $\Gamma_j = \Gamma_0 + \tilde{\Gamma}_j$, where $\tilde{\Gamma}_j$ denotes the collective decay induced by the dissipative interaction H'_{w} . The numerators in Eqs. (4) and (5) characterize the overlaps of photon modes and eigenmodes of the effective Hamiltonian in the transmission and reflection processes. The topological feature of the array is imprinted in the spatial profile of the eigenvectors, $|\psi_j^R\rangle$ and $|\psi_j^L\rangle$, and the structure of the spectrum, which eventually determines the photon transport. In Fig. 1(c), we show the transmission spectra for $d = \lambda_0/4, \lambda_0/2$ and $3\lambda_0/4$. The different linewidths of the transmission at $\omega = 0$ are determined by the decay rate of the edge mode. When the incident photon is resonant with the bulk states of frequency around $\pm 2J_0$, dips appear in the transmission spectra.

Nonreciprocal reflection.—Single-photon scattering by the topological atom array depends on the atomic spacing d and the direction of the incident photon. In Fig. 2(a), we show the transmission and reflection spectra for the left- and right-incident photons, where the transmission is reciprocal. However, reflections for the left- and right-incident photons are different, when the incident photon is resonant with the edge state. We define the reflection nonreciprocity

$$\Delta R = |R_l - R_r|, \quad (6)$$

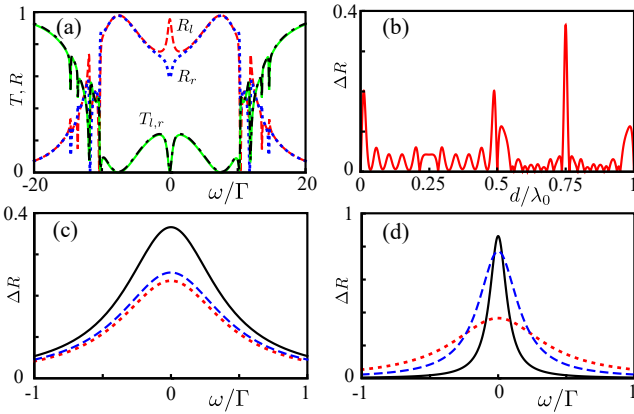


FIG. 2. (a) Transmission and reflection of a single photon through a topological atom array. Red-dashed (black-dot-dashed) and blue-dotted (green-solid) curves denote reflection (transmission) for left- and right-incident photons, respectively. Reflections from left and right are different at resonance. (b) Nonreciprocity at resonance changes with atomic spacing. The atom array with spacing $d = 3\lambda_0/4$ has the largest nonreciprocity for given parameters. (c) Nonreciprocity for topological arrays with different φ . Red-dotted, blue-dashed and black-solid curves correspond to $\varphi = 0.01\pi, 0.15\pi$ and 0.3π . (d) Nonreciprocity for topological arrays with different sizes. Red-dotted, blue-dashed and black-solid curves correspond to arrays with 11, 15 and 21 atoms. We consider $\varphi = 0.3\pi$ in (a,b,d); $d = 3\lambda_0/4$ in (a,c,d); atom number $N = 11$ in (a,b,c). Other parameters for all these figures: $J_0/\Gamma = 8$, $\Gamma_0/\Gamma = 0.05$.

where $R_l = |r_l|^2$ and $R_r = |r_r|^2$, with r_l (r_r) being the reflection amplitude for the left- (right-) incident photon. In Fig. 2(b) we show the nonreciprocal reflection for various atomic spacings. For $0 \leq d/\lambda_0 \leq 0.5$, the nonreciprocity is symmetric around $d = \lambda_0/4$, while for $0.5 \leq d/\lambda_0 \leq 1$ the nonreciprocity is symmetric around $d = 3\lambda_0/4$. The reflection is reciprocal for $d = 0, \lambda_0/2, \lambda_0$; and the maximal reflection nonreciprocity is found at $d = 3\lambda_0/4$. To study how the edge state affects the nonreciprocity, Fig. 2(c) shows ΔR for different values of φ . As φ increases, the nonreciprocity is enhanced. In Fig. 2(d), we consider the array with different numbers of atoms, showing that the longer the array the larger the nonreciprocity. Since J_0 controls the bandgap [85], we study the effect of the bandgap to the nonreciprocity by plotting ΔR versus the spacing d and the coupling strength J_0 in Fig. 3(a). As expected, for vanishing J_0 , the reflection is reciprocal. As J_0 increases, the position of the spacing d at which the maximal nonreciprocity appears changes accordingly. For relatively large J_0 , the maximal nonreciprocity appears at $d = 3\lambda_0/4$, which we refer as “magic spacing”.

In Fig. 3(b), the red dot-dashed (red-solid) and blue-dotted (blue-dashed) curves represent the reflections of the left- and right-incident photons for an array of size $N = 11$ ($N = 21$) and lattice spacing $d = 3\lambda_0/4$. Here,

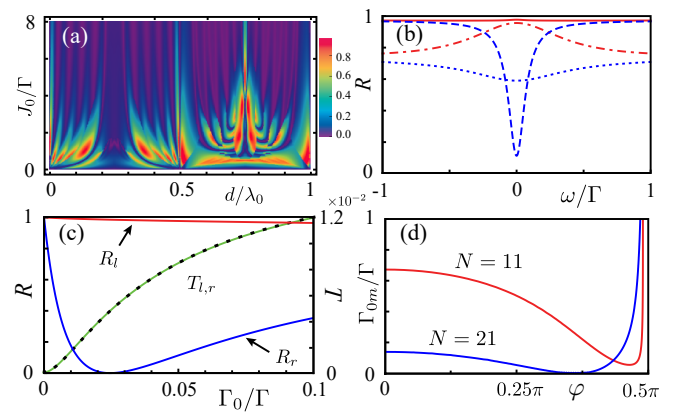


FIG. 3. (a) Nonreciprocity changes with atomic spacing d and coupling parameter J_0 . When J_0 is zero, there is no nonreciprocity. When J_0 is large, the nonreciprocity has a maximum at $d = 3\lambda_0/4$. (b) Nonreciprocal reflection: red-dot-dashed (red-solid) and blue-dotted (blue-dashed) curves are reflections for left- and right-incident photons with $N = 11$ ($N = 21$). (c) Reflections and transmissions for left- and right-incident photons change with Γ_0 . The reflection for right-incident photon R_r (blue-solid) is sensitive to Γ_0 and reduces to zero when $\Gamma_0 \simeq 0.0246$. The transmissions for left- and right-incident photons, denoted respectively by green-solid and black-dotted curves, are the same. (d) Parameter Γ_{0m} , defined by $R_r(\Gamma = \Gamma_{0m}) = 0$, versus φ . We consider $J_0/\Gamma = 8, d = 3\lambda_0/4$ in (b,c,d), $\varphi = 0.3\pi$ in (a,b,c), $\Gamma_0/\Gamma = 0.05$ in (a,b). In addition, $N = 11$ and $N = 21$ are studied in (a,c), respectively.

the reflection of the left-incident photon at resonance is almost unchanged as N increases, while the reflection of the right-incident photon is drastically reduced. For the right-incident photon, the reflection reduction has a non-trivial relation with the free space decay Γ_0 . As shown by the transmission and reflection versus Γ_0 in Fig. 3(c), the reciprocity of the reflection for $\Gamma_0 = 0$ results from time-reversal symmetry. When Γ_0 increases, in contrast to the almost unchanged reflection of the left-incident photon, the reflection of right-incident photon exhibits non-monotonic behavior, which reaches its minimum at Γ_{0m} . The minimum Γ_{0m} versus φ is plotted in Fig. 3(d) for $N = 11$ and 21. As N increases, Γ_{0m} is reduced; namely, a tiny free space decay is able to yield huge nonreciprocity. In addition, the transmissions of left- and right-incident photons are reciprocal and slightly changed as Γ_0 varies.

Quantum interference between waves reflected by edge and bulk modes.—The nonreciprocity originates from the inversion symmetry breaking due to the edge mode and the time-reversal symmetry breaking induced by the free space decay. For the magic spacing $d = 3\lambda_0/4$ and $0 \leq \varphi < \pi/2$, the edge mode appears on the left boundary. The left-incident photon barely couples to the edge mode; however, the right-incident photon strongly couples to the edge mode, which can be seen from the interaction

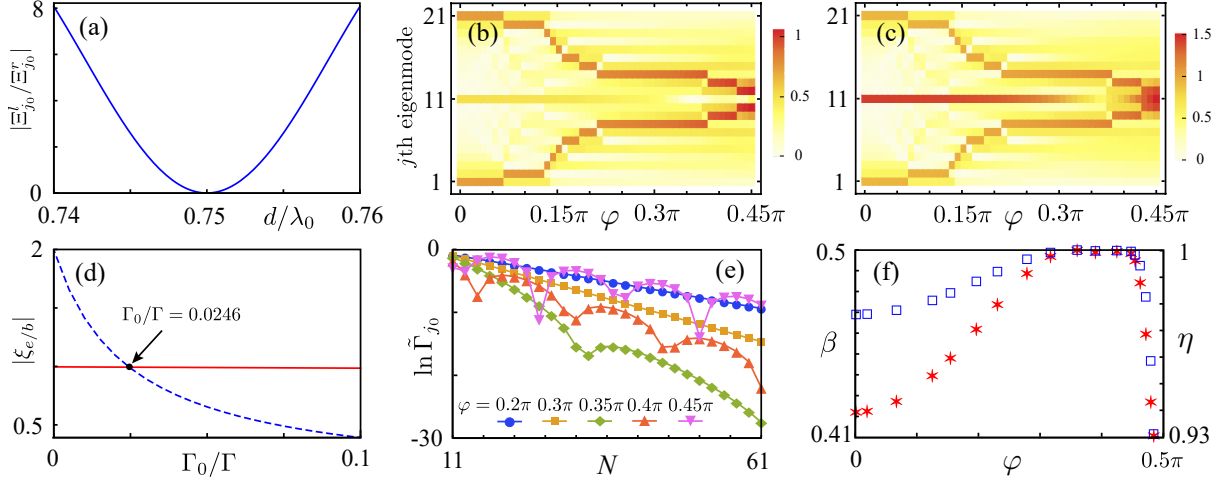


FIG. 4. (a) Relative strength for edge state reflecting photons coming from left and right directions. For given parameters, it has a minimum at $d = 3\lambda_0/4$. (b) and (c) represent $|\xi_j|$ ($j = 1, 2, \dots, N$) for photons coming from left and right, respectively. The vertical axis labels eigenmodes of H_{eff} . (d) Absolute values of $\xi_e = \xi_{j_0}$ (blue-dashed) and $\xi_b = \sum_{j \neq j_0} \xi_j$ (red-solid), which correspond to the edge mode and bulk modes, for the right-incident photon. (e) The scaling behaviors between $\ln \tilde{\Gamma}_{j_0}$ and N at different φ . (f) The β factor of edge state (blue square), and photon loss η (red star) for right-incident photon. We consider $J_0/\Gamma = 8$, $d = 3\lambda_0/4$ for (a,...,f), $\varphi = 0.3\pi$ for (a,d), $N = 21$ for (a,b,c,d,f), $\Gamma_0/\Gamma = 0.05$ for (a,b,c,e,f).

spectra

$$\Xi_j = \mathbf{V}^T |\psi_j^R\rangle \langle \psi_j^L| \mathbf{V}, \quad (7)$$

$$\tilde{\Xi}_j = \mathbf{V}^\dagger |\psi_j^R\rangle \langle \psi_j^L| \mathbf{V}, \quad (8)$$

i.e., the numerators in Eqs. (4) and (5), representing the amplitudes of reflection and transmission produced by the j th mode. It turns out that for vanishing direct interactions, i.e., $J_0 = 0$, Ξ_j ($\tilde{\Xi}_j$) are the same for the left- and right-incident photons. In Fig. 4(a), we show $|\Xi_{j_0}^l / \Xi_{j_0}^r|$ as a function of d , where j_0 denotes the edge state and l (r) represents the left- (right-) incident photon. It is clear that $|\Xi_{j_0}^l / \Xi_{j_0}^r|$ has a minimum at $d = 3\lambda_0/4$, which implies small overlap of the left-propagating photon and the edge mode at $d = 3\lambda_0/4$. (The parameters $\tilde{\Xi}_j$ in Eq. (S10) for the transmission process are found to be reciprocal with different atomic spacings [87]).

Even though the left-incident photon does not couple to the edge mode, it is totally reflected by the detuned bulk modes. For the right-incident photon, due to the finite coupling to the edge mode, the interference of waves reflected by the edge mode and bulk modes gives rise to the left outgoing wave. The contributions from the edge mode and bulk modes to the reflection can be characterized via

$$\xi_j = \frac{\Xi_j \Gamma}{-\Delta_j + i(\Gamma_0 + \tilde{\Gamma}_j)}, \quad (9)$$

where the incident photon is assumed to resonate with the edge state. In Figs. 4(b,c), the absolute values of different components ξ_j explicitly show the tiny and large

contributions from the edge mode for the left- and right-incident photons, respectively. In Fig. 4(d), absolute values of the contributions $\xi_e = \xi_{j_0}$ (blue-dashed) for the edge mode and $\xi_b = \sum_{j \neq j_0} \xi_j$ (red-solid) for bulk modes are shown for the right-incident photon at $\varphi = 0.3\pi$. For a closed system without free-space decay, the contributions from the edge mode and bulk modes are $\xi_e = 2e^{i\phi_0}$ and $\xi_b = -e^{i\phi_0}$, respectively, with $\phi_0 = \pi/2$. When the free-space decay Γ_0 is turned on, the reflection $\xi_b \sim -e^{i\phi_0}$ from bulk states is hardly affected by the small Γ_0 , since $|\Delta_{j \neq j_0}|$ or $\tilde{\Gamma}_{j \neq j_0}$ are much larger than Γ_0 . However, because the edge mode has zero energy at the magic spacing and a tiny decay rate $\tilde{\Gamma}_{j_0}$, the small free-space decay drastically reduces the reflection $\xi_e = e^{i\phi_0}$ from the edge mode by half when $\Gamma_0 = \tilde{\Gamma}_{j_0}$, which induces a vanishing reflection $\xi_e + \xi_b \sim 0$ and the maximal nonreciprocity. Accordingly, components of the edge state and bulk states are equal and the largest nonreciprocity takes place around $\varphi = 0.26\pi$ and 0.425π for Fig. 4(c) [87]. The waveguide-induced collective decay rate for the edge state at magic spacing exhibits a scaling $\tilde{\Gamma}_{j_0} \sim e^{-\nu N}$ for some values of φ , as shown in Fig. 4(e). Due to this scaling behavior, $\Gamma_{0m} \sim \tilde{\Gamma}_{j_0}$ decreases as the size of the array increases, in good agreement with Fig. 3(d).

Quantum scattering by edge and bulk modes yields anomalous photon transport. We introduce the beta factor [89, 90] $\beta = \tilde{\Gamma}_{j_0}/(\tilde{\Gamma}_{j_0} + \Gamma_0)$ to characterize the photon decay from the edge mode to the waveguide. In waveguide QED systems, atoms with high beta factor emit photons into the waveguide [91–93]. Our study shows that the photon in the waveguide totally emits to

free space even with $\beta \sim 1/2$ due to the interference with the reflective wave from bulk modes. In Fig. 4(f), we show the beta factor of the edge state and the photon loss $\eta = 1 - T_r - R_r$ from the waveguide to the free space for the right-incident photon, where $N = 21$. As presented in Fig. 4(f), when φ changes, the decay rate of the edge mode approaches the free-space decay and the β factor reaches 1/2, giving rise to an enhanced photon loss close to unity.

Implementation.—The waveguide QED with a topological atom array can be implemented in different experimental platforms, e.g., superconducting quantum circuits [94–96]. Recently, waveguide QED with multiple superconducting artificial atoms has made enormous progress in experiments [93, 97–101]. A topological array with tunable interactions of atoms has been implemented with superconducting quantum circuits [54]. In our system, the nonreciprocity originates from the inversion symmetry breaking and the free-space decay of atoms, as shown in Fig. 3(c). To observe the nonreciprocity in experiments, one can tune the coupling parameter φ , such that the position of Γ_{0m} shifts (see Fig. 3(d)) and the nonreciprocity changes accordingly. The nonreciprocal reflection also exists for the photon resonant with bulk modes [87]. However, due to the fact that the edge mode is topologically protected, for the incident photon resonant with the edge mode, the observation of the nonreciprocity in the reflection spectra is more feasible.

Discussions and Conclusions.—In this work, we study the photon scattering of a 1D waveguide coupled to a topological atom array. We find that the photon reflection by the topological atom array is nonreciprocal. It is attributed to destructive quantum interference between electromagnetic waves reflected by edge and bulk modes in the atom array. We show that, for the topological atom array with large bandgap, the nonreciprocity is maximal at a magic atomic spacing $d = 3\lambda_0/4$. The anomalous photon transport, i.e., the giant loss of the photon in the waveguide to free space, takes place, in spite of the relative decay $\Gamma/\Gamma_0 \gg 1$. Our work demonstrates the importance of topology in light-matter interacting phenomena, and sheds new light on topology-controlled quantum photonics.

Acknowledgments—W.N. thanks Prof. J.-M. Raimond for helpful discussions. Y.X.L. is supported by the Key-Area Research and Development Program of GuangDong Province under Grant No. 2018B030326001, the National Basic Research Program (973) of China under Grant No. 2017YFA0304304, and NSFC under Grant No. 11874037. W.N. was supported by the Tsinghua University Postdoctoral Support Program. T.S. acknowledges the support of NSFC No. 11974363. F.N. is supported in part by: NTT Research, Army Research Office (ARO) Grant No. W911NF-18-1-0358, Japan Science and Technology Agency (JST) through the CREST Grant No. JPMJCR1676, Japan Society

for the Promotion of Science (JSPS) (via the KAKENHI Grant No. JP20H00134, and the JSPS-RFBR Grant No. JPJSBP120194828), and the Grant No. FQXi-IAF19-06 from the Foundational Questions Institute (FQXi), a donor advised fund of the Silicon Valley Community Foundation.

* tshi@itp.ac.cn

† yuxiliu@mail.tsinghua.edu.cn

- [1] P. Lodahl, S. Mahmoodian, S. Stobbe, A. Rauschenbeutel, P. Schneeweiss, J. Volz, H. Pichler, and P. Zoller, *Chiral quantum optics*, *Nature* **541**, 473 (2017).
- [2] D. Roy, C. M. Wilson, and O. Firstenberg, *Colloquium: Strongly interacting photons in one-dimensional continuum*, *Rev. Mod. Phys.* **89**, 021001 (2017).
- [3] D. E. Chang, J. S. Douglas, A. González-Tudela, C.-L. Hung, and H. J. Kimble, *Colloquium: Quantum matter built from nanoscopic lattices of atoms and photons*, *Rev. Mod. Phys.* **90**, 031002 (2018).
- [4] J.-T. Shen and S. Fan, *Coherent Single Photon Transport in a One-Dimensional Waveguide Coupled with Superconducting Quantum Bits*, *Phys. Rev. Lett.* **95**, 213001 (2005).
- [5] D. E. Chang, A. S. Sørensen, E. A. Demler, and M. D. Lukin, *A single-photon transistor using nanoscale surface plasmons*, *Nat. Phys.* **3**, 807 (2007).
- [6] L. Zhou, Z. R. Gong, Y.-X. Liu, C. P. Sun, and F. Nori, *Controllable scattering of a single photon inside a one-dimensional resonator waveguide*, *Phys. Rev. Lett.* **101**, 100501 (2008).
- [7] L. Zhou, H. Dong, Y.-X. Liu, C. P. Sun, and F. Nori, *Quantum supercavity with atomic mirrors*, *Phys. Rev. A* **78**, 063827 (2008).
- [8] L. Zhou, S. Yang, Y.-X. Liu, C. P. Sun, and F. Nori, *Quantum Zeno switch for single-photon coherent transport*, *Phys. Rev. A* **80**, 062109 (2009).
- [9] G. Romero, J. J. García-Ripoll, and E. Solano, *Microwave Photon Detector in Circuit QED*, *Phys. Rev. Lett.* **102**, 173602 (2009).
- [10] J.-Q. Liao, Z. R. Gong, L. Zhou, Y.-X. Liu, C. P. Sun, and F. Nori, *Controlling the transport of single photons by tuning the frequency of either one or two cavities in an array of coupled cavities*, *Phys. Rev. A* **81**, 042304 (2010).
- [11] D. Witthaut and A. S. Sørensen, *Photon scattering by a three-level emitter in a one-dimensional waveguide*, *New J. Phys.* **12**, 043052 (2010).
- [12] H. Zheng, D. J. Gauthier, and H. U. Baranger, *Waveguide QED: Many-body bound-state effects in coherent and Fock-state scattering from a two-level system*, *Phys. Rev. A* **82**, 063816 (2010).
- [13] C.-H. Yan, L.-F. Wei, W.-Z. Jia, and J.-T. Shen, *Controlling resonant photonic transport along optical waveguides by two-level atoms*, *Phys. Rev. A* **84**, 045801 (2011).
- [14] B. Peropadre, J. Lindkvist, I.-C. Hoi, C. Wilson, J. J. Garcia-Ripoll, P. Delsing, and G. Johansson, *Scattering of coherent states on a single artificial atom*, *New J. Phys.* **15**, 035009 (2013).
- [15] Z. H. Wang, L. Zhou, Y. Li, and C. P. Sun, *Controllable single-photon frequency converter via a one-dimensional*

waveguide, *Phys. Rev. A* **89**, 053813 (2014).

[16] W. Z. Jia, Y. W. Wang, and Y.-X. Liu, *Efficient single-photon frequency conversion in the microwave domain using superconducting quantum circuits*, *Phys. Rev. A* **96**, 053832 (2017).

[17] T. Shi, Y. Chang, and J. J. García-Ripoll, *Ultrastrong Coupling Few-Photon Scattering Theory*, *Phys. Rev. Lett.* **120**, 153602 (2018).

[18] T. Li, A. Miranowicz, X. Hu, K. Xia, and F. Nori, *Quantum memory and gates using a Λ -type quantum emitter coupled to a chiral waveguide*, *Phys. Rev. A* **97**, 062318 (2018).

[19] G. Calajó, Y.-L. L. Fang, H. U. Baranger, and F. Ciccarello, *Exciting a Bound State in the Continuum through Multiphoton Scattering Plus Delayed Quantum Feedback*, *Phys. Rev. Lett.* **122**, 073601 (2019).

[20] O. V. Astafiev, A. A. Abdumalikov, A. M. Zagoskin, Y. A. Pashkin, Y. Nakamura, and J. S. Tsai, *Ultimate On-Chip Quantum Amplifier*, *Phys. Rev. Lett.* **104**, 183603 (2010).

[21] I.-C. Hoi, T. Palomaki, J. Lindkvist, G. Johansson, P. Delsing, and C. M. Wilson, *Generation of Nonclassical Microwave States Using an Artificial Atom in 1D Open Space*, *Phys. Rev. Lett.* **108**, 263601 (2012).

[22] Z. H. Peng, S. E. de Graaf, J. S. Tsai, and O. V. Astafiev, *Tunable on-demand single-photon source in the microwave range*, *Nat. Commun.* **7**, 1 (2016).

[23] P. Forn-Díaz, J. J. García-Ripoll, B. Peropadre, J.-L. Orgiazzi, M. A. Yurtalan, R. Belyansky, C. M. Wilson, and A. Lupascu, *Ultrastrong coupling of a single artificial atom to an electromagnetic continuum in the nonperturbative regime*, *Nat. Phys.* **13**, 39 (2017).

[24] A. P. Foster, D. Hallett, I. V. Iorsh, S. J. Sheldon, M. R. Godslan, B. Royall, E. Clarke, I. A. Shelykh, A. M. Fox, M. S. Skolnick, I. E. Itskevich, and L. R. Wilson, *Tunable Photon Statistics Exploiting the Fano Effect in a Waveguide*, *Phys. Rev. Lett.* **122**, 173603 (2019).

[25] T. S. Tsoi and C. K. Law, *Quantum interference effects of a single photon interacting with an atomic chain inside a one-dimensional waveguide*, *Phys. Rev. A* **78**, 063832 (2008).

[26] K. Lalumière, B. C. Sanders, A. F. van Loo, A. Fedorov, A. Wallraff, and A. Blais, *Input-output theory for waveguide QED with an ensemble of inhomogeneous atoms*, *Phys. Rev. A* **88**, 043806 (2013).

[27] D. Reitz, C. Sayrin, B. Albrecht, I. Mazets, R. Mitsch, P. Schneeweiss, and A. Rauschenbeutel, *Backscattering properties of a waveguide-coupled array of atoms in the strongly nonparaxial regime*, *Phys. Rev. A* **89**, 031804 (2014).

[28] F. Le Kien and A. Rauschenbeutel, *Propagation of nanofiber-guided light through an array of atoms*, *Phys. Rev. A* **90**, 063816 (2014).

[29] A. González-Tudela, V. Paulisch, D. E. Chang, H. J. Kimble, and J. I. Cirac, *Deterministic Generation of Arbitrary Photonic States Assisted by Dissipation*, *Phys. Rev. Lett.* **115**, 163603 (2015).

[30] M.-T. Cheng, J. Xu, and G. S. Agarwal, *Waveguide transport mediated by strong coupling with atoms*, *Phys. Rev. A* **95**, 053807 (2017).

[31] G.-Z. Song, E. Munro, W. Nie, F.-G. Deng, G.-J. Yang, and L.-C. Kwek, *Photon scattering by an atomic ensemble coupled to a one-dimensional nanophotonic waveguide*, *Phys. Rev. A* **96**, 043872 (2017).

[32] S. Mahmoodian, M. Čepulkovskis, S. Das, P. Lodahl, K. Hammerer, and A. S. Sørensen, *Strongly Correlated Photon Transport in Waveguide Quantum Electrodynamics with Weakly Coupled Emitters*, *Phys. Rev. Lett.* **121**, 143601 (2018).

[33] I. M. Mirza, J. G. Hoskins, and J. C. Schotland, *Dimer chains in waveguide quantum electrodynamics*, *Opt. Commun.* **463**, 125427 (2020).

[34] T. Caneva, M. T. Manzoni, T. Shi, J. S. Douglas, J. I. Cirac, and D. E. Chang, *Quantum dynamics of propagating photons with strong interactions: a generalized input-output formalism*, *New J. Phys.* **17**, 113001 (2015).

[35] T. Shi, D. E. Chang, and J. I. Cirac, *Multiphoton-scattering theory and generalized master equations*, *Phys. Rev. A* **92**, 053834 (2015).

[36] J. Ruostekoski and J. Javanainen, *Emergence of correlated optics in one-dimensional waveguides for classical and quantum atomic gases*, *Phys. Rev. Lett.* **117**, 143602 (2016).

[37] A. F. Kockum, G. Johansson, and F. Nori, *Decoherence-Free Interaction between Giant Atoms in Waveguide Quantum Electrodynamics*, *Phys. Rev. Lett.* **120**, 140404 (2018).

[38] Y. Chang, Z. R. Gong, and C. P. Sun, *Multiatom mirror for perfect reflection of single photons in a wide band of frequency*, *Phys. Rev. A* **83**, 013825 (2011).

[39] D. E. Chang, L. Jiang, A. Gorshkov, and H. Kimble, *Cavity QED with atomic mirrors*, *New J. Phys.* **14**, 063003 (2012).

[40] Z. Liao, X. Zeng, S.-Y. Zhu, and M. S. Zubairy, *Single-photon transport through an atomic chain coupled to a one-dimensional nanophotonic waveguide*, *Phys. Rev. A* **92**, 023806 (2015).

[41] R. J. Bettles, S. A. Gardiner, and C. S. Adams, *Cooperative eigenmodes and scattering in one-dimensional atomic arrays*, *Phys. Rev. A* **94**, 043844 (2016).

[42] Y. Ke, A. V. Poshakinskiy, C. Lee, Y. S. Kivshar, and A. N. Poddubny, *Inelastic Scattering of Photon Pairs in Qubit Arrays with Subradiant States*, *Phys. Rev. Lett.* **123**, 253601 (2019).

[43] R. Mitsch, C. Sayrin, B. Albrecht, P. Schneeweiss, and A. Rauschenbeutel, *Quantum state-controlled directional spontaneous emission of photons into a nanophotonic waveguide*, *Nat. Commun.* **5**, 1 (2014).

[44] R. Jones, G. Buonaiuto, B. Lang, I. Lesanovsky, and B. Olmos, *Collectively Enhanced Chiral Photon Emission from an Atomic Array near a Nanofiber*, *Phys. Rev. Lett.* **124**, 093601 (2020).

[45] N. Gheeraert, S. Kono, and Y. Nakamura, *Bidirectional emitter and receiver of itinerant microwave photons in a waveguide*, *arXiv:2004.01924* (2020).

[46] S. Okaba, T. Takano, F. Benabid, T. Bradley, L. Vincetti, Z. Maizelis, V. Yampol'skii, F. Nori, and H. Katori, *Lamb-Dicke spectroscopy of atoms in a hollow-core photonic crystal fibre*, *Nat. Commun.* **5**, 1 (2014).

[47] A. Goban, C.-L. Hung, J. D. Hood, S.-P. Yu, J. A. Muniz, O. Painter, and H. J. Kimble, *Superradiance for Atoms Trapped along a Photonic Crystal Waveguide*, *Phys. Rev. Lett.* **115**, 063601 (2015).

[48] N. V. Corzo, B. Gouraud, A. Chandra, A. Goban, A. S. Sheremet, D. V. Kupriyanov, and J. Laurat, *Large Bragg Reflection from One-Dimensional Chains of Trapped Atoms Near a Nanoscale Waveguide*, *Phys. Rev.*

Lett. **117**, 133603 (2016).

[49] H. L. Sørensen, J.-B. Béguin, K. W. Kluge, I. Iakouporov, A. S. Sørensen, J. H. Müller, E. S. Polzik, and J. Appel, *Coherent Backscattering of Light Off One-Dimensional Atomic Strings*, Phys. Rev. Lett. **117**, 133604 (2016).

[50] P. Solano, P. Barberis-Blostein, F. K. Fatemi, L. A. Orozco, and S. L. Rolston, *Super-radiance reveals infinite-range dipole interactions through a nanofiber*, Nat. Commun. **8**, 1 (2017).

[51] M. W. Johnson, M. H. Amin, S. Gildert, T. Lanting, F. Hamze, N. Dickson, R. Harris, A. J. Berkley, J. Johansson, P. Bunyk, E. M. Chapple, C. Enderud, J. P. Hilton, K. Karimi, E. Ladizinsky, N. Ladizinsky, T. Oh, I. Perminov, C. Rich, M. C. Thom, E. Tolkacheva, C. J. S. Truncik, S. Uchaikin, J. Wang, B. Wilson, and G. Rose, *Quantum annealing with manufactured spins*, Nature **473**, 194 (2011).

[52] R. Barends, A. Shabani, L. Lamata, J. Kelly, A. Mezzacapo, U. Las Heras, R. Babbush, A. G. Fowler, B. Campbell, Y. Chen, Z. Chen, B. Chiaro, A. Dunsworth, E. Jeffrey, E. Lucero, A. Megrant, J. Y. Mutus, M. Neeley, C. Neill, P. J. J. O’Malley, C. Quintana, P. Roushan, D. Sank, A. Vainsencher, J. Wenner, T. C. White, E. Solano, H. Neven, and J. M. Martinis, *Digitized adiabatic quantum computing with a superconducting circuit*, Nature **534**, 222 (2016).

[53] D.-W. Wang, C. Song, W. Feng, H. Cai, D. Xu, H. Deng, H. Li, D. Zheng, X. Zhu, H. Wang, S.-Y. Zhu, and M. O. Scully, *Synthesis of antisymmetric spin exchange interaction and chiral spin clusters in superconducting circuits*, Nat. Phys. **15**, 382 (2019).

[54] W. Cai, J. Han, F. Mei, Y. Xu, Y. Ma, X. Li, H. Wang, Y. P. Song, Z.-Y. Xue, Z.-q. Yin, S. Jia, and L. Sun, *Observation of Topological Magnon Insulator States in a Superconducting Circuit*, Phys. Rev. Lett. **123**, 080501 (2019).

[55] W. Nie, Z. H. Peng, F. Nori, and Y.-X. Liu, *Topologically Protected Quantum Coherence in a Superatom*, Phys. Rev. Lett. **124**, 023603 (2020).

[56] I. S. Besedin, M. A. Gorlach, N. N. Abramov, I. Tsitsilin, I. N. Moskalenko, A. A. Dobronosova, D. O. Moskalev, A. R. Matanin, N. S. Smirnov, I. A. Rodionov, A. N. Poddubny, and A. V. Ustinov, *Topological photon pairs in a superconducting quantum metamaterial*, arXiv:2006.12794 (2020).

[57] D. Marcos, P. Widmer, E. Rico, M. Hafezi, P. Rabl, U.-J. Wiese, and P. Zoller, *Two-dimensional lattice gauge theories with superconducting quantum circuits*, Ann. Phys. **351**, 634 (2014).

[58] A. Mezzacapo, E. Rico, C. Sabín, I. L. Egusquiza, L. Lamata, and E. Solano, *Non-Abelian $SU(2)$ Lattice Gauge Theories in Superconducting Circuits*, Phys. Rev. Lett. **115**, 240502 (2015).

[59] Y. Ando, *Topological insulator materials*, J. Phys. Soc. Jpn. **82**, 102001 (2013).

[60] J. K. Pachos, *Introduction to Topological Quantum Computation* (Cambridge University Press, 2012).

[61] M. Bello, G. Platero, J. I. Cirac, and A. González-Tudela, *Unconventional quantum optics in topological waveguide QED*, Sci. Adv. **5**, eaaw0297 (2019).

[62] C. A. Downing, T. J. Sturges, G. Weick, M. Stobińska, and L. Martín-Moreno, *Topological Phases of Polaritons in a Cavity Waveguide*, Phys. Rev. Lett. **123**, 217401 (2019).

[63] T. Haug, L. Amico, L.-C. Kwek, W. J. Munro, and V. M. Bastidas, *Topological pumping of quantum correlations*, Phys. Rev. Research **2**, 013135 (2020).

[64] E. Kim, X. Zhang, V. S. Ferreira, J. Bunker, J. K. Iverson, A. Sipahigil, M. Bello, A. Gonzalez-Tudela, M. Mirhosseini, and O. Painter, *Quantum electrodynamics in a topological waveguide*, arXiv:2005.03802 (2020).

[65] L. Leonforte, A. Carollo, and F. Ciccarello, *Vacancy-like dressed states in topological waveguide QED*, arXiv:2007.02949 (2020).

[66] F. D. M. Haldane and S. Raghu, *Possible Realization of Directional Optical Waveguides in Photonic Crystals with Broken Time-Reversal Symmetry*, Phys. Rev. Lett. **100**, 013904 (2008).

[67] S. Raghu and F. D. M. Haldane, *Analogs of quantum-Hall-effect edge states in photonic crystals*, Phys. Rev. A **78**, 033834 (2008).

[68] L. Lu, J. D. Joannopoulos, and M. Soljačić, *Topological photonics*, Nat. Photonics **8**, 821 (2014).

[69] K. Y. Bliokh, D. Smirnova, and F. Nori, *Quantum spin Hall effect of light*, Science **348**, 1448 (2015).

[70] K. Y. Bliokh, F. J. Rodríguez-Fortuño, F. Nori, and A. V. Zayats, *Spin-orbit interactions of light*, Nat. Photonics **9**, 796 (2015).

[71] K. Y. Bliokh, D. Leykam, M. Lein, and F. Nori, *Topological non-Hermitian origin of surface Maxwell waves*, Nat. Commun. **10**, 1 (2019).

[72] T. Ozawa, H. M. Price, A. Amo, N. Goldman, M. Hafezi, L. Lu, M. C. Rechtsman, D. Schuster, J. Simon, O. Zilberberg, and I. Carusotto, *Topological photonics*, Rev. Mod. Phys. **91**, 015006 (2019).

[73] Z. Wang, Y. D. Chong, J. D. Joannopoulos, and M. Soljačić, *Reflection-Free One-Way Edge Modes in a Gyromagnetic Photonic Crystal*, Phys. Rev. Lett. **100**, 013905 (2008).

[74] L. Lu, L. Fu, J. D. Joannopoulos, and M. Soljačić, *Weyl points and line nodes in gyroid photonic crystals*, Nat. Photonics **7**, 294 (2013).

[75] C. He, X.-C. Sun, X.-P. Liu, M.-H. Lu, Y. Chen, L. Feng, and Y.-F. Chen, *Photonic topological insulator with broken time-reversal symmetry*, Proc. Natl. Acad. Sci. U.S.A. **113**, 4924 (2016).

[76] T. Shi, H. Kimble, and J. I. Cirac, *Topological phenomena in classical optical networks*, Proc. Natl. Acad. Sci. U.S.A. **114**, E8967 (2017).

[77] D. Leykam, S. Mittal, M. Hafezi, and Y. D. Chong, *Reconfigurable Topological Phases in Next-Nearest-Neighbor Coupled Resonator Lattices*, Phys. Rev. Lett. **121**, 023901 (2018).

[78] K. Fang, Z. Yu, and S. Fan, *Realizing effective magnetic field for photons by controlling the phase of dynamic modulation*, Nat. Photonics **6**, 782 (2012).

[79] A. B. Khanikaev, S. H. Mousavi, W.-K. Tse, M. Kargarian, A. H. MacDonald, and G. Shvets, *Photonic topological insulators*, Nat. Mater. **12**, 233 (2013).

[80] M. C. Rechtsman, J. M. Zeuner, Y. Plotnik, Y. Lumer, D. Podolsky, F. Dreisow, S. Nolte, M. Segev, and A. Szameit, *Photonic Floquet topological insulators*, Nature **496**, 196 (2013).

[81] M. Hafezi, S. Mittal, J. Fan, A. Migdall, and J. Taylor, *Imaging topological edge states in silicon photonics*, Nat. Photonics **7**, 1001 (2013).

[82] O. Zilberberg, S. Huang, J. Guglielmon, M. Wang, K. P. Chen, Y. E. Kraus, and M. C. Rechtsman, *Photonic topological boundary pumping as a probe of 4D quantum*

Hall physics, *Nature* **553**, 59 (2018).

[83] Y. Yang, Z. Gao, H. Xue, L. Zhang, M. He, Z. Yang, R. Singh, Y. Chong, B. Zhang, and H. Chen, *Realization of a three-dimensional photonic topological insulator*, *Nature* **565**, 622 (2019).

[84] W. P. Su, J. R. Schrieffer, and A. J. Heeger, *Solitons in Polyacetylene*, *Phys. Rev. Lett.* **42**, 1698 (1979).

[85] W. Nie and Y.-X. Liu, *Bandgap-assisted quantum control of topological edge states in a cavity*, *Phys. Rev. Research* **2**, 012076 (2020).

[86] A. Gonzalez-Tudela, D. Martin-Cano, E. Moreno, L. Martin-Moreno, C. Tejedor, and F. J. Garcia-Vidal, *Entanglement of Two Qubits Mediated by One-Dimensional Plasmonic Waveguides*, *Phys. Rev. Lett.* **106**, 020501 (2011).

[87] See Supplemental Material for additional details.

[88] D. C. Brody, *Biorthogonal quantum mechanics*, *J. Phys. A* **47**, 035305 (2013).

[89] V. S. C. Manga Rao and S. Hughes, *Single quantum-dot Purcell factor and β factor in a photonic crystal waveguide*, *Phys. Rev. B* **75**, 205437 (2007).

[90] G. Lecamp, P. Lalanne, and J. P. Hugonin, *Very Large Spontaneous-Emission β Factors in Photonic-Crystal Waveguides*, *Phys. Rev. Lett.* **99**, 023902 (2007).

[91] M. Arcari, I. Söllner, A. Javadi, S. Lindskov Hansen, S. Mahmoodian, J. Liu, H. Thyrrstrup, E. H. Lee, J. D. Song, S. Stobbe, and P. Lodahl, *Near-Unity Coupling Efficiency of a Quantum Emitter to a Photonic Crystal Waveguide*, *Phys. Rev. Lett.* **113**, 093603 (2014).

[92] A. B. Young, A. C. T. Thijssen, D. M. Beggs, P. Androvitsaneas, L. Kuipers, J. G. Rarity, S. Hughes, and R. Oulton, *Polarization Engineering in Photonic Crystal Waveguides for Spin-Photon Entanglers*, *Phys. Rev. Lett.* **115**, 153901 (2015).

[93] M. Mirhosseini, E. Kim, X. Zhang, A. Sipahigil, P. B. Dieterle, A. J. Keller, A. Asenjo-Garcia, D. E. Chang, and O. Painter, *Cavity quantum electrodynamics with atom-like mirrors*, *Nature* **569**, 692 (2019).

[94] J. You and F. Nori, *Atomic physics and quantum optics using superconducting circuits*, *Nature* **474**, 589 (2011).

[95] X. Gu, A. F. Kockum, A. Miranowicz, Y.-X. Liu, and F. Nori, *Microwave photonics with superconducting quantum circuits*, *Phys. Rep.* **718-719**, 1 (2017).

[96] I. Carusotto, A. A. Houck, A. J. Kollár, P. Roushan, D. I. Schuster, and J. Simon, *Photonic materials in circuit quantum electrodynamics*, *Nat. Phys.* **16**, 268 (2020).

[97] A. F. Van Loo, A. Fedorov, K. Lalumiere, B. C. Sanders, A. Blais, and A. Wallraff, *Photon-mediated interactions between distant artificial atoms*, *Science* **342**, 1494 (2013).

[98] B. Kannan, M. Ruckriegel, D. Campbell, A. F. Kockum, J. Braumüller, D. Kim, M. Kjaergaard, P. Krantz, A. Melville, B. M. Niedzielski, A. Vepsäläinen, R. Winik, J. Yoder, F. Nori, T. P. Orlando, S. Gustavsson, and W. D. Oliver, *Waveguide quantum electrodynamics with superconducting artificial giant atoms*, *Nature* **583**, 775 (2020).

[99] B. Kannan, D. Campbell, F. Vasconcelos, R. Winik, D. Kim, M. Kjaergaard, P. Krantz, A. Melville, B. M. Niedzielski, J. Yoder, T. P. Orlando, S. Gustavsson, and W. D. Oliver, *Generating Spatially Entangled Itinerant Photons with Waveguide Quantum Electrodynamics*, *arXiv:2003.07300* (2020).

[100] A. M. Vadraj, A. Ask, T. G. McConkey, I. Nsanzineza, C. W. Chang, A. F. Kockum, and C. M. Wilson, *Engineering the Level Structure of a Giant Artificial Atom in Waveguide Quantum Electrodynamics*, *arXiv:2003.14167* (2020).

[101] J. D. Brehm, A. N. Poddubny, A. Stehli, T. Wolz, H. Rotzinger, and A. V. Ustinov, *Waveguide Bandgap Engineering with an Array of Superconducting Qubits*, *arXiv:2006.03330* (2020).

TOPOLOGY-CONTROLLED NONRECIPROCAL PHOTON SCATTERING IN A WAVEGUIDE:
SUPPLEMENTAL MATERIAL

I. Waveguide-mediated edge state

In the main text, we consider the effective Hamiltonian $H_{\text{eff}} = H_{\text{SSH}} + H'$. The Hamiltonian of the topological atom array is

$$H_{\text{SSH}} = \left(J_- \sum_{i=\text{odd}} \sigma_i^+ \sigma_{i+1}^- + J_+ \sum_{i=\text{even}} \sigma_i^+ \sigma_{i+1}^- \right) + \text{H.c.}, \quad (\text{S1})$$

with $J_{\mp} = J_0(1 \mp \cos \varphi)$. When the array has an odd number of atoms, only one edge state exists. The Hamiltonian can be diagonalized as $H_{\text{SSH}} = \sum_{j=1}^N \varepsilon_j |\alpha_j\rangle \langle \alpha_j|$, with $\varepsilon_{j-1} \leq \varepsilon_j \leq \varepsilon_{j+1}$. We assume that $j = j_0$ represents the edge state. In Fig. S1(a), we show the energy spectrum of H_{SSH} .

The edge state is localized to the left (right) boundary of the atom array for $0 \leq \varphi < 0.5\pi$ ($0.5\pi < \varphi \leq \pi$). The left edge state is $|\alpha_{j_0}\rangle = \frac{1}{N} \sum_{i=\text{odd}} (-J_-/J_+)^{\frac{i-1}{2}} |i\rangle$ with $|i\rangle = \sigma_i^+ |G\rangle$. And the right edge state is $|\alpha_{j_0}\rangle = \frac{1}{N} \sum_{i=\text{odd}} (-J_-/J_+)^{\frac{N-i}{2}} |i\rangle$. Here, $|G\rangle$ is the ground state of the atom array. In Fig. S1(b), we present wave functions of edge states at $\varphi = 0.3\pi$ and $\varphi = 0.7\pi$. They are symmetric to each other about the center of the atom array. Without loss of generality, we study the topological atom array with a left-localized edge state, i.e., $0 \leq \varphi < 0.5\pi$.

In addition to the SSH interaction, the waveguide can induce indirect interactions between atoms. By taking into account the atomic dissipation to free space, we obtain

$$H' = -i\Gamma_0 \sum_i \sigma_i^+ \sigma_i^- - i\Gamma \sum_{ij} \cos(k_0|x_i - x_j|) \sigma_i^+ \sigma_j^- + \Gamma \sum_{ij} \sin(k_0|x_i - x_j|) \sigma_i^+ \sigma_j^-. \quad (\text{S2})$$

At $J_0 \gg \Gamma$, the edge state is protected by the bandgap and is weakly perturbed by the waveguide-mediated interactions. The effective edge state can be approximately written as

$$|\psi_{j_0}^R\rangle \approx |\alpha_{j_0}\rangle + \sum_{j \neq j_0} \frac{\langle \alpha_j | H' | \alpha_{j_0} \rangle}{\varepsilon_{j_0} - \varepsilon_j} |\alpha_j\rangle, \quad (\text{S3})$$

and

$$\langle \psi_{j_0}^L | \approx \langle \alpha_{j_0} | + \sum_{j \neq j_0} \frac{\langle \alpha_{j_0} | H' | \alpha_j \rangle}{\varepsilon_{j_0} - \varepsilon_j} \langle \alpha_j |. \quad (\text{S4})$$

Here, $|\psi_{j_0}^R\rangle$ and $\langle \psi_{j_0}^L |$ are the right and left vectors of the edge mode in the effective Hamiltonian H_{eff} , respectively. Because of the non-Hermitian Hamiltonian H' , we know that $|\psi_{j_0}^R\rangle \neq |\psi_{j_0}^L\rangle$, but $\langle \psi_{j_0}^L | \psi_{j_0}^R \rangle = 1$. We can know from Eqs. (S3) and (S4) that the effective edge mode contains components of the bulk modes.

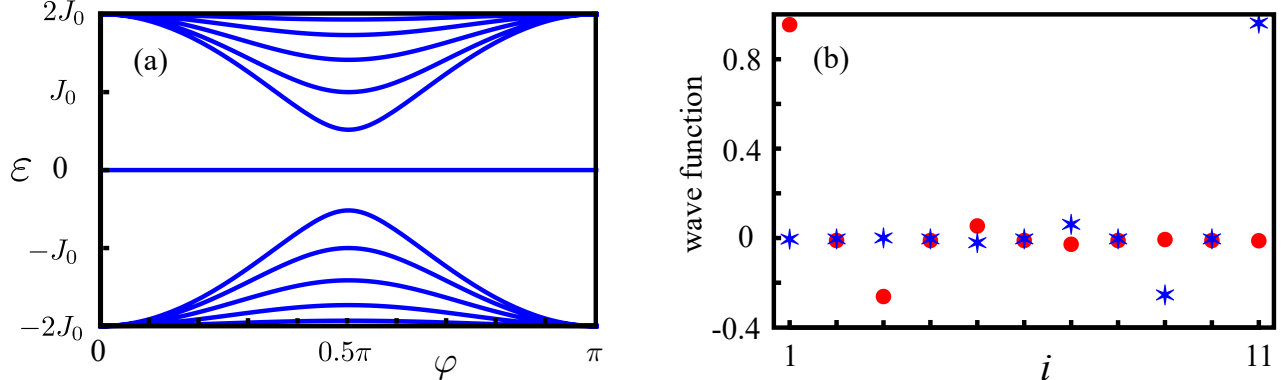


FIG. S1. (a) Energy spectrum of H_{SSH} . (b) Wave function of edge state at $\varphi = 0.3\pi$ (red-dotted) and $\varphi = 0.7\pi$ (blue-starred). Here, we consider atom number $N = 11$.

II. Single-photon scattering by a topological atom array

A. Photon scattering by a many-body quantum system

In this subsection, we present formulas for photon scattering by an atom array. The single-photon scattering by a many-body system in a waveguide can be studied using Green's function [S1]. The amplitudes of reflection and transmission for a single photon are respectively

$$r = -i\Gamma \mathbf{V}^T \mathbf{G} \mathbf{V}, \quad (\text{S5})$$

$$t = 1 - i\Gamma \mathbf{V}^\dagger \mathbf{G} \mathbf{V}, \quad (\text{S6})$$

with Green's function

$$\mathbf{G} = \frac{1}{\omega - H_{\text{eff}}}. \quad (\text{S7})$$

We consider the spectrum decomposition $H_{\text{eff}} = \sum_j (\Delta_j - i\tilde{\Gamma}_j) |\psi_j^R\rangle\langle\psi_j^L|$, where $|\psi_j^R\rangle$ and $\langle\psi_j^L|$ are the right and left vectors of the j th mode. For simplicity, we assume that $j = 1, 2, \dots, N$, label the eigenmodes of H_{eff} with ascending order of energy Δ_j ; and $j = j_0$ represents the edge state. Note that $|\psi_j^R\rangle$ and $\langle\psi_j^L|$ form a biorthogonal basis with $\langle\psi_j^L|\psi_{j'}^R\rangle = \delta_{jj'}$. Therefore, the reflection and transmission amplitudes can be written as

$$r(\omega) = -i\Gamma \sum_j \frac{\mathbf{V}^T |\psi_j^R\rangle\langle\psi_j^L| \mathbf{V}}{\omega - \Delta_j + i\tilde{\Gamma}_j}, \quad (\text{S8})$$

$$t(\omega) = 1 - i\Gamma \sum_j \frac{\mathbf{V}^\dagger |\psi_j^R\rangle\langle\psi_j^L| \mathbf{V}}{\omega - \Delta_j + i\tilde{\Gamma}_j}. \quad (\text{S9})$$

The above equations show how the eigenstates of the system (atom array + waveguide) scatter a single photon. The topological atom array coupled with the waveguide can be modelled as a superatom with multiple energy levels. We note that equations (S8) and (S9) can also be used to study photon scattering for a multilevel system without spatial extension, e.g., a three-level atom [S2], and giant atoms, which are nonlocally coupled to electromagnetic fields [S3]. From Eqs. (S8) and (S9) we know that photon reflection and transmission in the waveguide result from quantum interference between different scattering components, induced by eigenmodes of the effective Hamiltonian. Therefore, topological quantum systems, which have nontrivial spectrum structures and edge states, are of particular importance for scattering photons. In this work, we pinpoint the roles played by the bandgap and edge state in *nonreciprocal photon reflection*.

B. Nonreciprocal reflection controlled by bandgap and edge state

In the waveguide-coupled topological atom array studied in this work, photon transmission and reflection are respectively reciprocal and nonreciprocal when the edge state is resonantly driven. The difference of reciprocity for transmission and reflection comes from distinctive light-matter interactions in photon scattering processes. From Eqs. (S8) and (S9), scattering processes for reflection and transmission are characterized by

$$\Xi_j = \mathbf{V}^T |\psi_j^R\rangle\langle\psi_j^L| \mathbf{V}, \quad (\text{S10})$$

and

$$\tilde{\Xi}_j = \mathbf{V}^\dagger |\psi_j^R\rangle\langle\psi_j^L| \mathbf{V}. \quad (\text{S11})$$

Equations (S10) and (S11) represent light-matter interactions between propagating photons and eigenmodes in the topological atom array. From Eqs. (S3) and (S4), $|\psi_j^R\rangle\langle\psi_j^L|$ for the edge state can be approximately expressed as

$$|\psi_{j_0}^R\rangle\langle\psi_{j_0}^L| = |\alpha_{j_0}\rangle\langle\alpha_{j_0}| - \sum_{j \neq j_0} \frac{1}{\varepsilon_j} (\langle\alpha_j|H'|\alpha_{j_0}\rangle|\alpha_j\rangle\langle\alpha_{j_0}| + \langle\alpha_{j_0}|H'|\alpha_j\rangle|\alpha_{j_0}\rangle\langle\alpha_j|) + \dots \quad (\text{S12})$$

In the above equation, we assume that the bandgap of the topological atom array is large, i.e., $J_0 \gg \Gamma$ [S4]. Therefore, the waveguide produces effective couplings between edge state and bulk states. To study the role of modes in

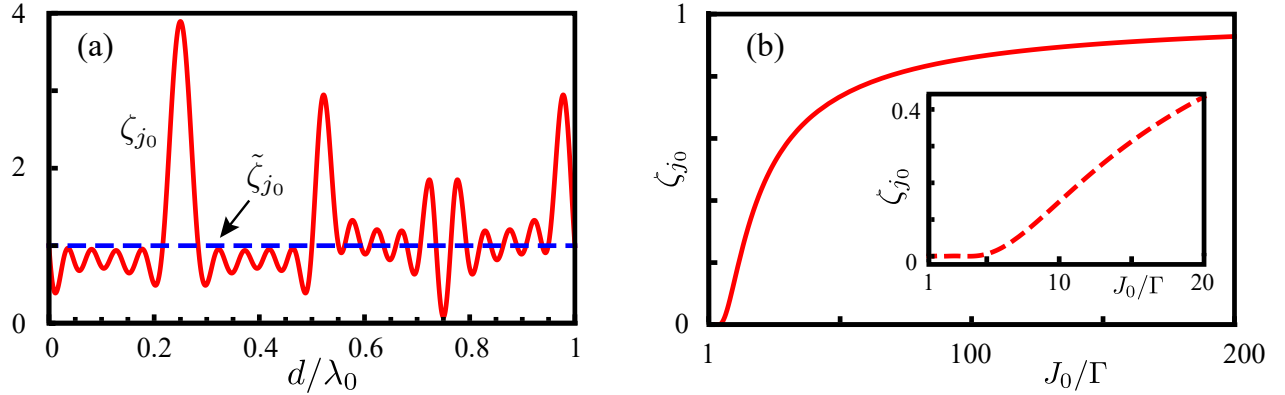


FIG. S2. (a) Reflection and transmission factors for edge state. Red-solid and blue-dashed curves correspond to reflection and transmission, respectively. Here, we consider the incident photon is resonant with the edge state and $J_0/\Gamma = 8$. (b) $|\zeta_{j_0}|$ for different values of J_0 with $d = 3\lambda_0/4$. As the increase of J_0 , $|\zeta_{j_0}|$ approaches one. Other parameters considered in (a) and (b) are: $\varphi = 0.3\pi$, $\Gamma_0/\Gamma = 0.05$ and atom number $N = 11$.

reflecting photons with different incident directions, we define relative strength of waves, which come from left and right directions, reflected by the j th eigenmode

$$\zeta_j = \frac{|\Xi_j^l|}{|\Xi_j^r|}, \quad (\text{S13})$$

where l and r label the left- and right-incident photons. Similarly, $\tilde{\zeta}_j = |\tilde{\Xi}_j^l/\tilde{\Xi}_j^r|$ uncovers the directionality of transmitted waves through the j th eigenmode. In Fig. S2(a), we present ζ_{j_0} and $\tilde{\zeta}_{j_0}$ for the edge state for different atomic spacings d . We can see that the ratio is the same for the transmission, but it is spacing-dependent for reflection. In particular, there is a minimum of ζ_{j_0} at $d = 3\lambda_0/4$. The difference between $\Xi_{j_0}^l$ and $\Xi_{j_0}^r$ makes the edge state critical in controlling photon transport in the waveguide. In Fig. S2(b), we present $|\zeta_{j_0}|$ changed with J_0 . When J_0 is large, ζ_{j_0} is close to one. Therefore, the bandgap should not be too large such that the waveguide-mediated edge-bulk couplings, i.e., the second term in Eq. (S12), are not negligible.

Photon reflection depends on several parameters of the topological atom array. In Fig. S3(a), we present the reflectional nonreciprocity for atom arrays with different sizes. The size affects nonreciprocity enormously. For a small atom array, the nonreciprocity is small at $\varphi = 0$ and increases as φ grows. However, when atom array is large, the nonreciprocity has a large value at $\varphi = 0$ and decreases with φ . When the atom array approaches the critical

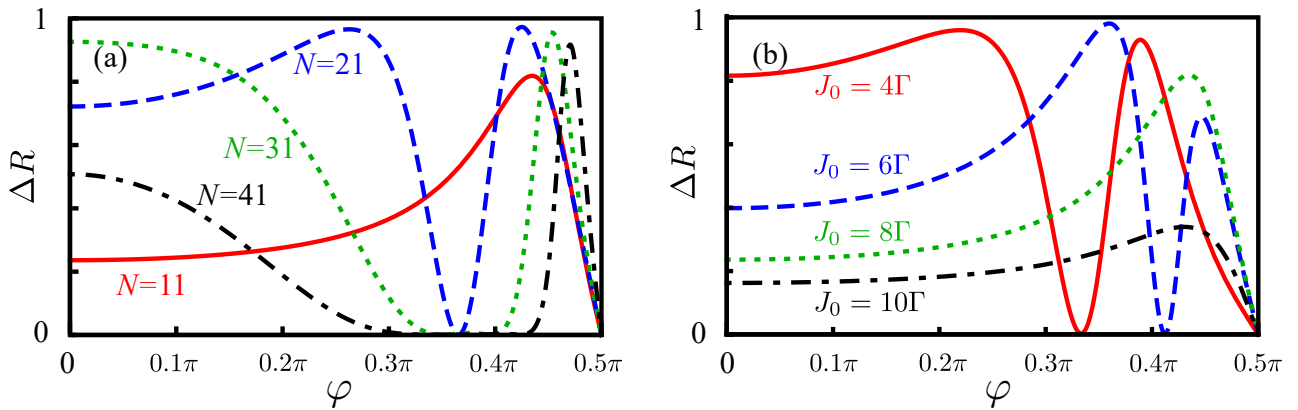


FIG. S3. (a) Reflectional nonreciprocity for different sizes of atom arrays. The red-solid, blue-dashed, green-dotted and black-dot-dashed curves correspond to arrays with atom numbers $N = 11, 21, 31$ and 41 . Here, we consider $J_0/\Gamma = 8$. (b) Reflectional nonreciprocity for different values of J_0 . The red-solid, blue-dashed, green-dotted and black-dot-dashed curves correspond to $J_0/\Gamma = 4, 6, 8$ and 10 . The atom number is assumed to be $N = 11$. Other parameters in (a) and (b) are: $d = 3\lambda_0/4$, $\Gamma_0/\Gamma = 0.05$.

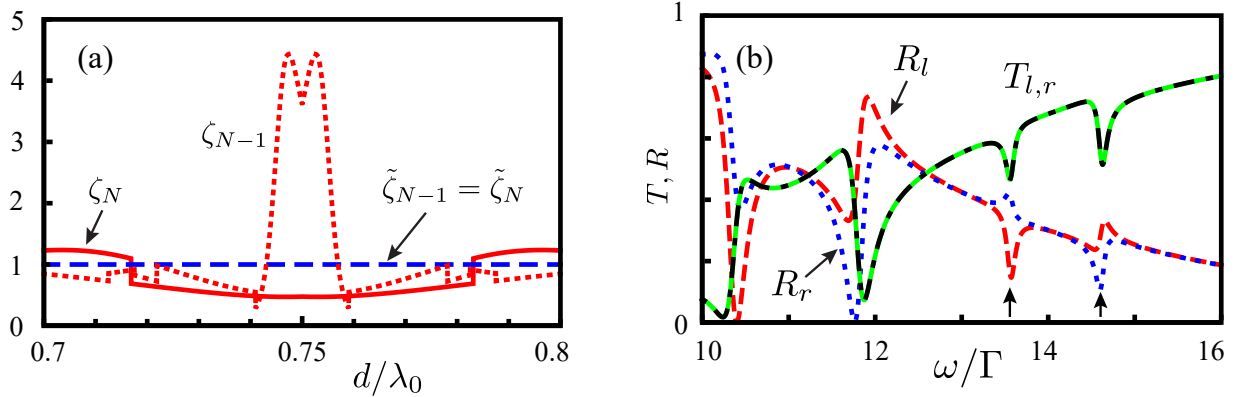


FIG. S4. (a) The parameters ζ_j with $j = N$ and $j = N - 1$ are represented by red-solid and red-dotted curves; $\tilde{\zeta}_j$ with $j = N$ and $N - 1$ are the same, as shown by the blue-dashed line. (b) Transmission and reflection of photons which drive bulk states. Transmissions are the same for left- and right-incident photons, which are represented by green-solid and black-dot-dashed curves. However, the reflections are different. The red-dashed and blue-dotted curves correspond to reflections for left- and right-incident photons. The arrows indicate modes with $j = N - 1$ and N .

point $\varphi = 0.5\pi$, the nonreciprocity is reduced to zero. In Fig. 4(c) in the main text, $|\xi_{j_0}|$ for the left-incident photon is reduced around $\varphi = 0.3\pi$ for $N = 21$. Accordingly, the nonreciprocity is reduced (see the blue-dashed curve in Fig. S3(a)). In particular, around $\varphi = 0.26\pi$ and 0.425π , the nonreciprocity reaches maximum. In Fig. S3(b), we study the effect of J_0 , which controls bandgap of the atom array. For relatively large values of J_0/Γ , the nonreciprocity ΔR is large at $\varphi = 0$. And the nonreciprocity can be tuned in a large regime by changing φ . However, as J_0 is increased, ΔR is reduced at $\varphi = 0$. The nonreciprocity is tunable in a small regime.

In the usual experiments with superconducting quantum circuits, the atom arrays have small sizes (around 10–20 qubits). One can obtain large reflectional nonreciprocity by choosing appropriate values of J_0 and φ .

C. Nonreciprocal reflection for photons resonant with bulk states

In the main text, we study nonreciprocal reflection for photons which are resonant with the edge state. From the analysis in the previous subsection, we know that the waveguide-induced interaction modifies the edge state and gives rise to distinctive reflections for photons with different incident directions. Similar to the edge state, bulk states in the topological atom array are also modified by waveguide-induced interaction. Therefore, nonreciprocal reflection can be found for photons whose frequencies are resonant with bulk states.

In Fig. S4(a), we show $|\zeta_j|$ for bulk states with $j = N - 1$ (red-dotted) and $j = N$ (red-solid). The bulk states with $j = N - 1$ and $j = N$ have different reflectional coefficients Ξ_j for left- and right-incident photons. However, the parameters $|\tilde{\zeta}_j|$ for $j = N - 1$ and $j = N$ are the same, as shown by the blue-dashed line. In Fig. S4(b), we show the transmission and reflection spectra. The transmission spectra are the same for left and right incident photons (green-solid and black-dot-dashed curves). But the reflection spectra are different. The arrows indicate bulk states with $j = N - 1$ and $j = N$. For the reason that frequencies between bulk states are small, it is challenging to observe reflectional nonreciprocity for photons with same frequencies as bulk states.

D. Γ_0 -dependent reflectional nonreciprocity

In the main text, we find that, with small Γ_0/Γ and large J_0/Γ , the reflectional nonreciprocity is maximal at $d = 3\lambda_0/4$. The atomic decay to free space Γ_0 alters the nonreciprocity. In Fig. S5(a), we compare reflections at $d = \lambda_0/4$ and $d = 3\lambda_0/4$ for different values of Γ_0/Γ . At $d = 3\lambda_0/4$, the large nonreciprocity can be found at small value of Γ_0/Γ , as we studied in the main text. The increase of Γ_0/Γ makes the nonreciprocity smaller. But for $d = \lambda_0/4$, a large nonreciprocity is found when Γ_0 is comparable with Γ . In Fig. S5(b), we show the nonreciprocity for $d = \lambda_0/4$ at different values of J_0 . Different from $d = 3\lambda_0/4$ (see Fig. S3), J_0 does not have significantly changes the nonreciprocity. In the main text, we have shown that paired bulk states attribute to photon scattering at $d = 3\lambda_0/4$.

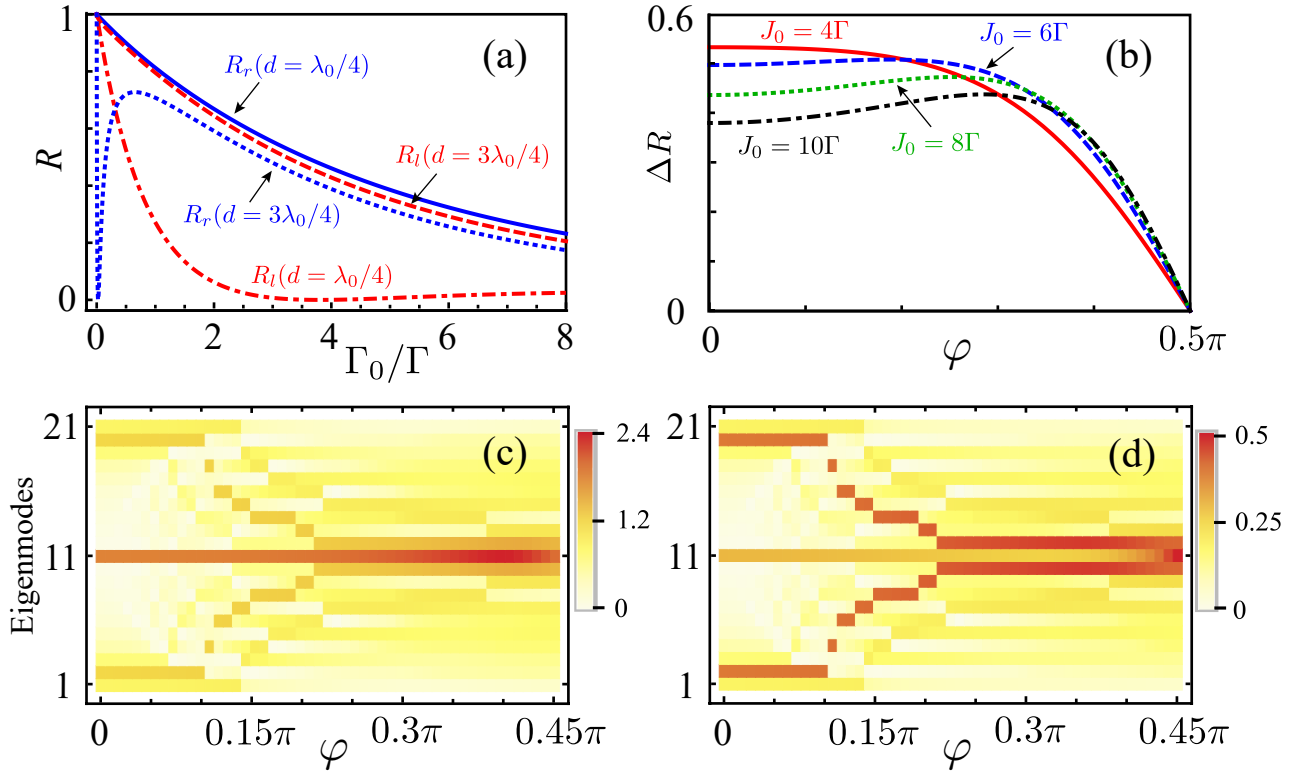


FIG. S5. (a) Photon reflections at different atomic spacings. Red-dot-dashed (red-dashed) and blue-solid (blue-dotted) curves denote reflections for photons coming from left and right at $d = \lambda_0/4$ ($d = 3\lambda_0/4$). Photon reflection for $d = \lambda_0/4$ has large nonreciprocity when Γ_0/Γ is large. Here, we consider $\varphi = 0.3\pi$. (b) Reflectional nonreciprocity changes with φ . Red-solid, blue-dot-dashed, green-dotted and black-dot-dashed curves correspond to $J_0/\Gamma = 4, 6, 8$ and 10 . (c) and (d) represent absolute values of ξ_j for photons coming from left and right, respectively. We consider $\Gamma_0/\Gamma = 2$ in (b)-(d), and the number of atoms $N = 21$ in (a)-(d).

A similar situation is found for $d = \lambda_0/4$, as presented in Figs. S5(c) and S5(d). When the parameter φ changes, different pairs of bulk states are coupled with propagating photons. For $d = 0, \lambda_0/2, \lambda_0$ or other values, pairs of bulk states do not contribute equally to photon scattering.

* tshi@itp.ac.cn

† yuxiliu@mail.tsinghua.edu.cn

[S1] T. Shi, D. E. Chang, and J. I. Cirac, *Multiphoton-scattering theory and generalized master equations*, *Phys. Rev. A* **92**, 053834 (2015).

[S2] D. Witthaut and A. S. Sørensen, *Photon scattering by a three-level emitter in a one-dimensional waveguide*, *New J. Phys.* **12**, 043052 (2010).

[S3] A. F. Kockum, G. Johansson, and F. Nori, *Decoherence-Free Interaction between Giant Atoms in Waveguide Quantum Electrodynamics*, *Phys. Rev. Lett.* **120**, 140404 (2018).

[S4] W. Nie and Y.-X. Liu, *Bandgap-assisted quantum control of topological edge states in a cavity*, *Phys. Rev. Research* **2**, 012076 (2020).